UNIVERSIDADE FEDERAL DO CARIRI
INSTITUTO DE FORMAÇÃO DE EDUCADORES
LICENCIATURA EM FÍSICA

CICERO DÁRIO GRANGEIRO PATRICIO

INVESTIGATING SOLAR CYCLES USING MATHEMATICAL MORPHOLOGY

BREJO SANTO
2026

CICERO DÁRIO GRANGEIRO PATRICIO

INVESTIGATING SOLAR CYCLES USING MATHEMATICAL MORPHOLOGY

Trabalho de Conclusão de Curso apresentado ao curso de Licenciatura em Física do Instituto de Formação de Educadores da Universidade Federal do Cariri, na modalidade de artigo aceito para publicação em periódico científico, como requisito parcial para obtenção do grau de Licenciado em Física.

Orientador: Prof. Dr. Gilson Francisco de Oliveira Junior.
Coorientador: Prof. Dr. Tharcísyo Sá e Sousa Duarte

BREJO SANTO

2026

Dados Internacionais de Catalogação na Publicação
Universidade Federal do Cariri
Sistema de Bibliotecas

P314i Patricio, Cicero Dario Grangeiro.
Investigating solar cycles using mathematical morphology/ Cicero Dário Grangeiro Patricio. – 2026.
21 f.: il. color.

Artigo Científico (Graduação em Licenciatura em Física) – Instituto de Formação de Educadores, Universidade Federal do Cariri, Brejo Santo, CE, 2026.

Orientador: Prof. Dr. Gilson Francisco de Oliveira Junior.
Coorientador: Prof. Dr. Tharcísyo Sá e Sousa Duarte.

Publicado originalmente em: Solar Physics (2026) 301:2
https://doi.org/10.1007/s11207-025-02598-7

1. Manchas solares. 2. Ciclo solar. 3. Morfologia matemática. 4. Processamento de imagens. 5. PyMoST. I. Oliveira Junior, Gilson Francisco de (Orient.). II. Duarte, Tharcísyo Sá e Sousa (Coorient.). III. Universidade Federal do Cariri. IV. Título.

CDD 523.74

Bibliotecário: João Bosco Dumont do Nascimento – CRB 3/1355

CICERO DÁRIO GRANGEIRO PATRICIO

INVESTIGATING SOLAR CYCLES USING MATHEMATICAL MORPHOLOGY

Trabalho de Conclusão de Curso apresentado ao curso de Licenciatura em Física do Instituto de Formação de Educadores da Universidade Federal do Cariri, na modalidade de artigo aceito para publicação em periódico científico, como requisito parcial para obtenção do grau de Licenciado em Física.

BANCA EXAMINADORA

Documento assinado digitalmente
GILSON FRANCISCO DE OLIVEIRA JUNIOR
Data: 31/08/2026 14:37:47-0300
Verifique em https://validar.iti.gov.br

Prof. Dr. Gilson Francisco de Oliveira Junior. (Orientador)
Universidade Federal do Cariri (UFCA)

Documento assinado digitalmente
THARCISYO SA E SOUSA DUARTE
Data: 31/08/2026 11:38:12-0300
Verifique em https://validar.iti.gov.br

Prof. Dr. Tharcísyo Sá e Sousa Duarte (Coorientador)
Universidade Federal do Cariri (UFCA)

Documento assinado digitalmente
RICARDO OLIVEIRA GONCALVES
Data: 31/08/2026 11:00:00-0300
Verifique em https://validar.iti.gov.br

Prof. Dr. Ricardo Oliveira Gonçalves
Universidade Federal do Cariri (UFCA)

Documento assinado digitalmente
JEFFERSON SOARES DA COSTA
Data: 27/08/2026 10:23:48-0300
Verifique em https://validar.iti.gov.br

Prof. Dr. Jefferson Soares da Costa
Universidade Federal do Rio Grande do Norte (UFRN)

BREJO SANTO, 31 DE JULHO DE 2026

Solar Physics (2026) 301:2
https://doi.org/10.1007/s11207-025-02598-7

RESEARCH

Investigating Solar Cycles Using Mathematical Morphology

Cicero D. Grangeiro[1] · Tharcisyo S.S. Duarte[1] · Jefferson S. da Costa[2] · Hugo R. Coelho[3] · Gilson F. de Oliveira Junior[1] · José-Dias do Nascimento Jr[3]

Received: 3 September 2024 / Accepted: 11 December 2025 / Published online: 5 January 2026

Abstract

In this study, we report on the processing and analysis of around 10,000 images of the solar disk, obtained from the SOHO and SDO satellites, available in the Helioviewer database. Using our own code, PyMoST (Python Morphological Sunspot Tracker), which employs a mathematical morphology technique, we were able to automatically track and analyze approximately 52,000 sunspots in these images, covering the period from January 1, 1998 to August 28, 2025. By using PyMoST we were able to obtain the distribution of the number of spots as a function of solar latitude and time, accurately reproducing Solar Cycles 23, 24 and the current phase of Solar Cycle 25, in agreement with the literature. In addition, our code was also able to determine the areas and number of sunspots, showing excellent correlation with the results reported by the Royal Greenwich Observatory (RGO), Kodaikanal Solar Observatory (KSO) and the International Sunspot Number - Solar Influences Data Analysis Center (SIDIC), thus consolidating the efficiency of our tool and its importance for the investigation of solar magnetic activity.

Keywords Sunspots · Solar cycle · Observations · Morphology · PyMoST

✉ C.D. Grangeiro
dario.grangeiro@aluno.ufca.edu.br

✉ T.S.S. Duarte
tharcisyo.duarte@ufca.edu.br

J.S. da Costa
jefferson.dacosta@ect.ufrn.br

H.R. Coelho
hugocoelho@fisica.ufrn.br

G.F. de Oliveira Junior
gilson.francisco@ufca.edu.br

J.-D. do Nascimento Jr
jdonascimento@fisica.ufrn.br

[1] Universidade Federal do Cariri, UFCA, Instituto de Formação de Educadores, IFE, 63260-000, Brejo Santo, Brazil

[2] Universidade Federal do Rio Grande do Norte, UFRN, Escola de Ciência e Tecnologia, ECT, 59078-970, Natal, Brazil

[3] Universidade Federal do Rio Grande do Norte, UFRN, Departamento De Física Teórica e Experimental, DFTE, 59072-970, Natal, Brazil

1. Introduction

Continuous observations of the Sun result in a vast and varied database, mainly consisting of images of the solar disk at multiple wavelengths. Automated analysis of this extensive dataset allows us to optimize the process of identifying and monitoring indicators of magnetic activity, such as sunspots. These spots are dark regions on the solar surface associated with intense magnetic fields. From this automated analysis, we are able to investigate the dynamics and behavior of the Sun's differential rotation and also contribute to the improvement of models related to solar activities and forecasting mechanisms for space weather (Vourlidas 2021).

The literature contains several studies on the automation process for identifying and analyzing sunspots. Zharkov et al. (2004) use a code in the IDL language to investigate white light images obtained by the SOHO Observatory, together with Ca II (k1) images from the Meudon Observatory in France. Goel and Mathew (2014) adopted a pre-developed method (Selective Binary and Gaussian Function Regularized Level Set - SBGFRLS), based on the concept of "on the level set", for the detection of spots in SOHO/MDI white light images. Curto, Blanca, and Martínez (2008), as well as Watson, Fletcher, and Marshall (2011), used tools based on mathematical morphology for the automated sunspot detection process. More recently, the Convolution Neural Network method has also been used in the process of recognizing and analyzing sunspots, as demonstrated in the works by Chola and Benifa (2022), Santos et al. (2023).

The use of the most varied techniques for observing and analyzing sunspots, either manual or automated, has enabled us to better understand the differential nature of solar rotation, the result of compiling several years of daily observations of magnetic activity through sunspots (Carrington 1863; Maunder 1903, 1904), which can be visualized in the classic butterfly diagram. This diagram shows the periodic pattern of the latitudinal movement of the spots on the solar disk, occurring approximately every 11 years, a period known as the spot cycle (Schwabe 1844). A longer cycle can also be observed, lasting around 22 years, characterizing the solar cycle (Hale et al. 1919). These patterns provide valuable insights into the dynamics and evolution of solar activity over time.

To study sunspots, we developed a code called PyMoST - Python Morphological Sunspot Tracker (Grangeiro 2025)[1] using the Python programming language and, based on the concepts of mathematical morphology, a shape-based image processing technique anchored in set theory. The main objective of PyMoST is to identify and track sunspots and analyze, in an automated way, their physical evolution over the last two solar cycles (Solar Cycles 23 and 24), as well as the evolutionary behavior of the current solar cycle (Solar Cycle 25). Through our code, we tried to reproduce Spörer's Law of Zones, using publicly available data from the NASA database to create Mauder's Butterfly Diagram for the respective cycles, validating the result with the diagrams from the Kodaikanal Solar Observatory (Mandal et al. 2017) and the Royal Greenwich Observatory (Hathaway 2015). We also aimed to analyze the characteristics of the cycle based on its fundamental elements, such as the area and number of sunspots, in order to gain a more detailed understanding of these solar phenomena. In this context, PyMoST is a powerful tool for monitoring and studying sunspots, with significant potential to contribute to the field of solar physics.

[1] https://github.com/grangeirodario/pymost.

2. Methodology

2.1. Data

The dataset employed in this study consists of publicly available solar disk images obtained from two distinct instruments: MDI (Michelson Doppler Imager) and HMI (Helioseismic and Magnetic Imager), onboard SOHO (Solar Heliospheric Observatory) and SDO (Solar Dynamics Observatory) satellites, respectively. These images are provided in JPEG2000 format through the Helioviewer database[1]

The first dataset was acquired with the MDI instrument via the hvpy DataSource MDI_INT (SOHO/MDI, continuum measurements) and spans the period from January 1, 1998, to December 6, 2010, consisting of grayscale images with a resolution of 1024 × 1024 pixels. The second dataset was obtained with the HMI instrument via the hvpy DataSource HMI_INT (SDO/HMI, continuum measurements), covering the period from December 6, 2010, to August 28, 2025. These images are also in grayscale but feature a substantially higher resolution of 4096 × 4096 pixels, thereby providing enhanced detail for the analysis.

Although the dataset used throughout the study relies primarily on Helioviewer JPEG2000 products, an additional verification was conducted to assess the equivalence between Helioviewer data and corresponding FITS files retrieved directly from JSOC. A detailed explanation of this validation, including the retrieval procedure and the comparative results obtained after applying the same processing pipeline, is provided in Appendix 4. This ensures that the choice of data source does not introduce systematic differences in the measurements derived for sunspot detection and characterization.

2.2. Mathematical Morphology

For the automated identification and tracking of sunspots, we adopted the image processing technique known as mathematical morphology. Introduced by Matheron (1975) and Serra (1982), mathematical morphology is a theory of non-linear transformations based on set theory that analyzes images according to the geometric shape of the structures that are present. This approach has proved effective in various applications, such as remote sensing (Banfield and Raftery 1992), medical field (Morales et al. 2013; Klingler et al. 1988; El Abbadi and Al Saadi 2013; Roslan, Jamil, and Mahmud 2010), detection and segmentation of urban objects (Serna and Marcotegui 2014) and, as explored in this paper, analysis of astronomical images, specifically images of the solar disk.

Mathematical morphology emerged in France in the mid-1960s, derived from the study of the geometry of porous media in images. G. Matheron and J. Serra were pioneers in applying set theory to the analysis of images, initially binary, considering porous media as binary sets, in which the matrix of points represented the object and the pores its complement. This approach made it possible to process objects in binary images using simple operations from the universe of set theory: union, intersection, complement and translation, paving the way for the development of mathematical morphology as a powerful tool in image processing (Soille et al. 1999; Bloch, Heijmans, and Ronse 2007; Haralick, Sternberg, and Zhuang 1987).

[1] Helioviewer.org is part of the Helioviewer Project, an open-source initiative for visualizing solar and heliospheric data, funded by ESA and NASA. The JPEG2000 files from Helioviewer include metadata that enables precise spatial positioning of the image data, allowing them to be processed and analyzed similarly to maps derived from FITS data (Mumford et al. 2015).

In general, morphological transformations are achieved by combining two basic operators, dilation and erosion (Soille et al. 1999; Bloch, Heijmans, and Ronse 2007). These combinations include the aperture and white top-hat transform used in this work. For a more in-depth understanding of the white top-hat morphological operator, see Section 4.5 of Soille et al. (1999) or Section 1.3.2 of Najman and Talbot (2013). With regard to this operator, it is necessary to understand the concept of structuring element and also the main morphological operators, as we will do below.

2.3. Structuring Element

With morphological operations, we aim to identify and extract relevant elements present in an image. To achieve this, we probe the image using another set of defined shape, known as the structuring element (Soille et al. 1999). The aim is to make a comparison between all the sets considered to be objects in an image and the structuring element previously selected. Based on this, we apply geometric transformations to simplify the objects in the images, preserving essential characteristics and eliminating irrelevant ones (Haralick, Sternberg, and Zhuang 1987; Bloch, Heijmans, and Ronse 2007). Irrelevant characteristics can be understood as noise in the captured image equipment caused by low-quality sensors, artifacts caused by errors in the processing of the captured image, or even structures that we want to remove, such as the complete background of images that can make it difficult to segment objects of interest.

The structuring element is a set of known and well-defined data, i.e. an arbitrary set, small in relation to the image, and predefined in shape. Their shape is tipically chosen based on prior knowledge of the geometry of the structures that are considered relevant or irrelevant in an image. The size and shape of the structuring element are very important for processing and must match the morphological characteristics of the objects to be processed in the image. For example, linear-shaped structuring elements are more suitable for extracting linear objects. Therefore, structuring elements are chosen based on three aspects: shape, dimension and directionality (Soille et al. 1999).

2.4. Morphological Operations

Mathematical morphology is fundamentally based on two primary operations: erosion and dilation. The formal mathematical framework for these operations is extensively detailed in Soille et al. (1999), Bloch, Heijmans, and Ronse (2007) and Najman and Talbot (2013). For this work, we adopt the definitions provided by Soille et al. (1999), where erosion is defined as follows: given a set X and a structuring element B, the erosion of X by B denoted as $\varepsilon_B(X)$ consists of the set of points x for which B is entirely contained within X when its origin is translated to position x. Erosion plays a crucial role in mathematical morphology, as it enlarges the background, reduces the size of objects in the image, and modifies concave corners, with the extent of these effects depending on the chosen structuring element.

Dilation is the complementary operation to erosion, forming the fundamental duality in mathematical morphology. As defined by Soille et al. (1999), the dilation of a set X by a structuring element B, denoted as $\delta_B(X)$, consists of the set of all points x where B intersects X when its origin is translated to position x. Given that dilation and erosion are dual operations, the properties of dilation naturally derive from those of erosion. While erosion reduces objects and expands the background, dilation has the opposite effect: it enlarges objects, diminishes the background, and modifies convex corners, with the extent of these transformations depending on the chosen structuring element.

Erosion and dilation are often combined to generate more advanced morphological transformations. One such transformation is morphological opening, which consists of applying erosion followed by dilation using the same structuring element. Since erosion reduces objects and modifies their shape in a non-reversible manner, morphological opening aims to restore as much of the original structure as possible while preserving the essential features of the objects (Soille et al. 1999). This operation is particularly useful for removing small noise, disconnecting thin structures that bridge separate objects, and smoothing object boundaries. When a disk-shaped structuring element is used, morphological opening effectively preserves the general size of objects while refining their contours (Bloch, Heijmans, and Ronse 2007).

The morphological transformations explored so far have been based on prior knowledge of the structural characteristics of the elements to be processed, a fundamental principle of mathematical morphology. However, the white top-hat transformation, or top-hat by opening, extends these possibilities by adopting a different approach. As described in Soille et al. (1999) and further emphasized by Najman and Talbot (2013), this technique applies morphological opening using a structuring element that does not match the relevant structures in the image, effectively filtering them out. The removed structures are then retrieved by computing the arithmetic difference between the original image and its opened version. This transformation is particularly useful for enhancing bright objects in varying backgrounds, isolating small features, and improving contrast in image analysis.

The white top-hat transformation is particularly useful in scenarios where distinguishing between relevant and irrelevant objects in an image is challenging. In many cases, it is more effective to remove significant structures from an image rather than attempting to eliminate background noise or irrelevant features (Soille et al. 1999). A practical example of this approach is found in white-light images of the solar disk. When the objective is to segment sunspots, it is more efficient to remove them from the solar disk rather than attempting to isolate them directly from the background. This methodology has been successfully applied in previous studies, such as Watson, Fletcher, and Marshall (2011), Carvalho et al. (2020), and more recently in Bourgeois et al. (2024), reinforcing its effectiveness in solar image processing.

2.5. Obtaining the Heliographic Coordinates of Sunspots from the White Top-Hat Transform

Segmenting sunspots in white-light images presents considerable challenges, especially differentiating between the spots on the solar disk and the outer dark region. The white top-hat transformation, as described by Najman and Talbot (2013), offers an effective solution to this problem, highlighting small features in images with background variations that could obscure important details, such as sunspots. In our study, we adopted this strategy for the accurate and efficient detection of sunspots, as detailed next.

First, we invert the original image, creating a negative image where the solar disk becomes dark, and the sunspots become light. We then adjust a structuring element to remove the sunspots through the morphological opening. Erosion, the first step of the opening, eliminates sunspots, but also alters the geometric characteristics of the image, especially the solar disk. To mitigate these alterations, we apply dilation, the second step of the opening, seeking to rebuild the original pattern of the features as much as possible. Finally, we recovered the sunspots by performing the arithmetic difference between the image resulting from the opening and the original negative image. This procedure, as discussed above, corresponds to the white top-hat transformation.

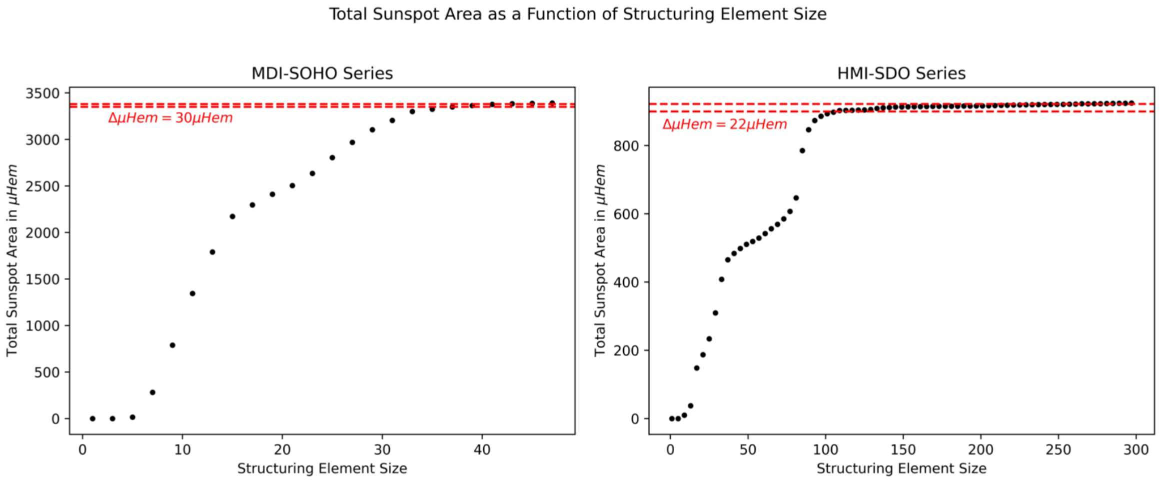

Figure 1 Scatter plots illustrating the relationship between structuring element size and total projected area for two solar datasets: MDI-SOHO (left) and HMI-SDO (right).

As we saw in Section 2.3 the choice of structuring element depends on the objective of the work, and in this case, it must be directly related to three aspects: shape, dimension and directionality. With regard to shape, Carvalho et al. (2020) emphasizes that the most suitable structuring element for sunspot analysis should be the disk structuring element. The justification is simple: morphological operators would alter the geometric shape of the solar disk if applied using structuring elements other than the disk element. Regarding the dimension, considering the aspects discussed in Soille et al. (1999), Bloch, Heijmans, and Ronse (2007), Haralick, Sternberg, and Zhuang (1987), Najman and Talbot (2013), it must be smaller than the image to be transformed to eliminate the sunspots present on the solar disk through the top-hat operator, so we chose an element that is slightly larger than the sunspots. As for directionality, the choice of the disk structuring element fits well because the features of interest, i.e. sunspots, are isotropic (Bourgeois et al. 2024).

With regard to the dimension of the structuring element, considering the aspects discussed in Soille et al. (1999), Bloch, Heijmans, and Ronse (2007), Haralick, Sternberg, and Zhuang (1987), Najman and Talbot (2013), it must be smaller than the image to be transformed and, in order to eliminate the sunspots present on the solar disk using the top-hat operator, it must be slightly larger than the sunspots. To find the ideal size threshold for extracting the sunspots, we calculated the total area of the sunspots as a function of the size of the structuring element, as shown in Figure 1.

The graph on the left shows the total area of sunspots as a function of the size of the structuring element in a SOHO-MDI image from September 26, 2001. It can be seen that the variation in area is minimal for structuring element values between 35 and 50 pixels, resulting in a difference of only $30\mu Hem$. Similarly, the graph on the right shows this relationship for an SDO-HMI image from April 6, 2013, where structuring element sizes between 100 and 300 pixels generate a variation of only $22\mu Hem$ in the total sunspot area.

So, following the procedure described above, we selected a disk-shaped structuring element for the white top-hat transform. To handle the two sets of data, we used two different sizes of the structuring element. For SOHO-MDI images (1024×1024 pixels), we apply a structuring element of size 45×45 pixels. For SDO-HMI images (4096×4096 pixels), we use a larger structuring element of 147×147 pixels. This adjustment in the size of the structuring element effectively addressed the differences in resolution, ensuring consistent performance of the transformation in both data sets. The dimensions were chosen as a value

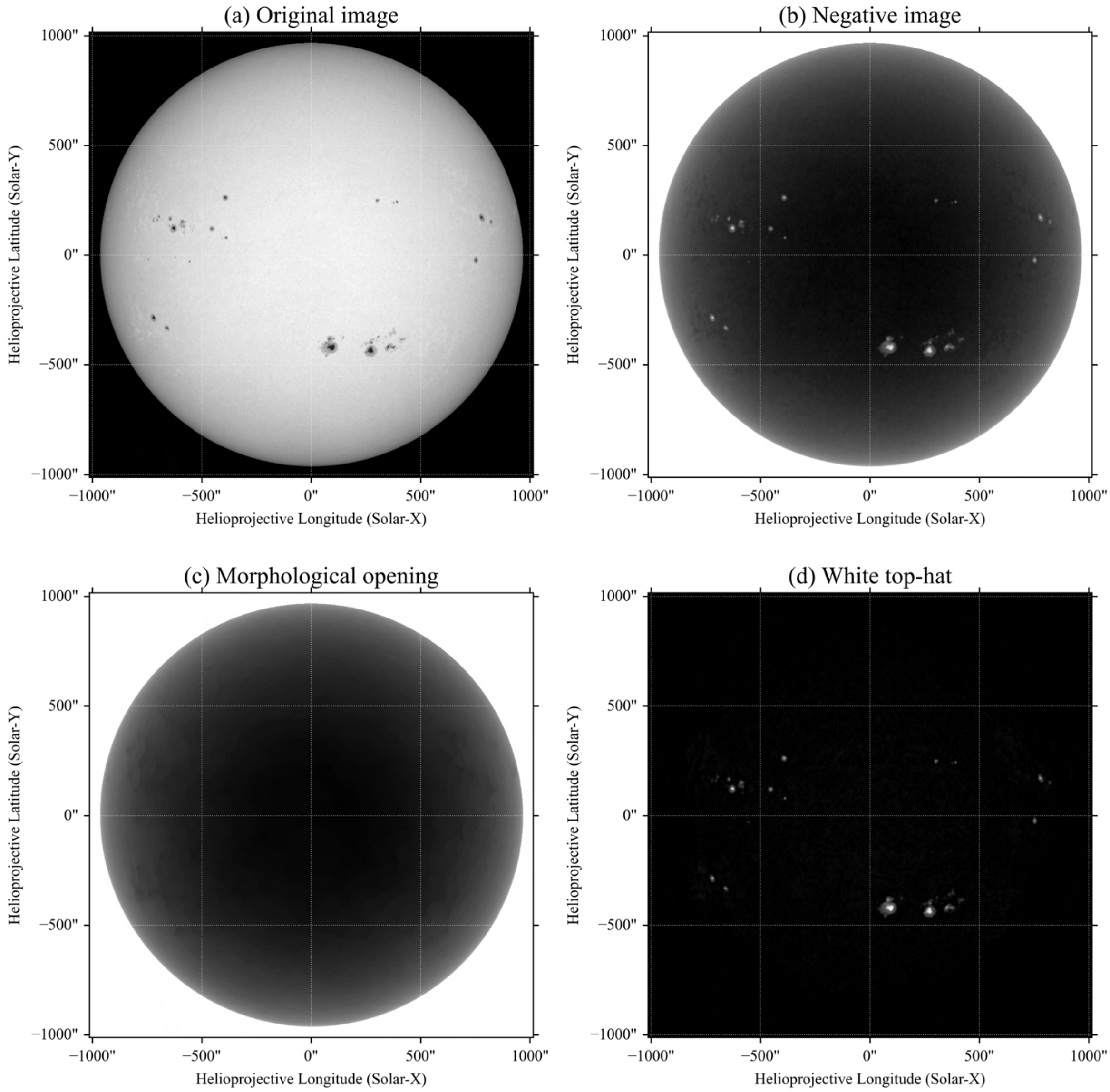

Figure 2 White top-hat transform in its stages: (a) original image of the solar disk, (b) image with inverted tonality, (c) morphological aperture and (d) transformed image.

close to the average between the structuring element values for which the projected area has the least variation.

When applying a white top-hat transformation to a white light image of the solar disk with inverted tonality, the result is an image that accentuates the intensity peaks on the disk, specifically highlighting sunspots and intensity boundaries. Figure 2 demonstrates this process. In Figure 2 (a), the original grayscale image, captured on September 26, 2001, is shown. Figure 2 (b) presents the negative image, where the solar disk appears dark and the sunspots are accentuated. A morphological opening (erosion followed by dilation) is then applied to this negative image, producing the result in Figure 2 (c), where the sunspots are removed, leaving only the background of the solar disk. Finally, by subtracting this background image from the original negative image, we obtain Figure 2 (d), where the sunspots are distinctly highlighted. This process effectively isolates the sunspots, eliminating the background, and making them easier to identify and analyze.

To accurately determine the heliographic coordinates of the sunspots, particularly their latitudes, we applied an inverted binarization to the images that had undergone the white top-hat transformation. This operation is designed to produce dark spots on a light background, thereby facilitating the identification and analysis of the sunspots. The process of inverse binarization can be mathematically defined as follows:

$$dst(x, y) = \begin{cases} 0 \text{ if } src(x, y) > \text{ thresh;} \\ (max_{val}) \text{ otherwise,} \end{cases} \tag{1}$$

where $dst(x, y)$ represents the resulting pixel intensity at position (x, y), $src(x, y)$ corresponds to the original pixel intensity at position (x, y) to be binarized, *thresh* is the defined threshold value and max_{val} denotes the maximum gray level value. In this process, any gray level above the threshold value is assigned a gray level of 0, while values below the threshold are assigned the maximum gray level. We apply binarization to eliminate residual noise remaining after the white top-hat transformation, to unify the umbra and penumbra regions of the sunspots for integrated tracking, and to merge smaller groups of spots into a single region. This approach simplifies the subsequent analysis and monitoring of the sunspots.

After binarization, we generated a map of the image by converting the pixel coordinate system to the Helioprojective Cartesian (HPC) system. We then identified and outlined all regions on the map where the tonal difference exceeded 255, corresponding to areas that represent sunspots against the background. For each sunspot detected, we calculated the centroid coordinates, representing the average position of the pixels constituting the sunspot. Finally, these HPC centroid coordinates were converted to the Stonyhurst Heliographic system, providing the latitude and longitude of the sunspots on the Sun's surface.

2.6. Obtaining the Area of Sunspots

In addition to determining the heliographic coordinates of the sunspots, we also estimated their areas, expressed in millionths of a solar hemisphere (μHem), from the regions delineated by the detected contours. For this purpose, each pixel belonging to the sunspot was treated individually, such that its projected area in the image was converted into a physical area on the solar surface, accounting for the geometric projection effect as a function of the pixel position relative to the center of the solar disk. This procedure follows the formulation proposed by Meadows (2002), defined as:

$$A_m = \frac{10^6}{2\pi R^2} \sum_{i=1}^{N} \frac{A_{\text{pix}}}{\cos \rho_i}, \tag{2}$$

where A_m denotes the total area of the sunspot in millionths of the Sun's visible hemisphere, A_{pix} corresponds to the area of a single pixel in the image (in squared pixels), R is the radius of the solar disk in pixels, and ρ_i is the angular distance on the solar surface between the disk center and the i-th pixel of the sunspot. In this way, the foreshortening correction was applied pixel by pixel, and only after this step were the corrected areas summed, yielding the final sunspot area expressed in μHem.

The white top-hat transformation, inverted binarization, and calculation of the sunspot areas were implemented using functions from the OpenCV library (Bradski 2000). The generation of the solar disk image map and the conversions between coordinate systems were carried out using the SunPy (The SunPy Community et al. 2020; Mumford et al. 2025) and Astropy (Price-Whelan et al. 2018) libraries, respectively. For more in-depth information on coordinate systems in solar images, refer to the work of Thompson (2006).

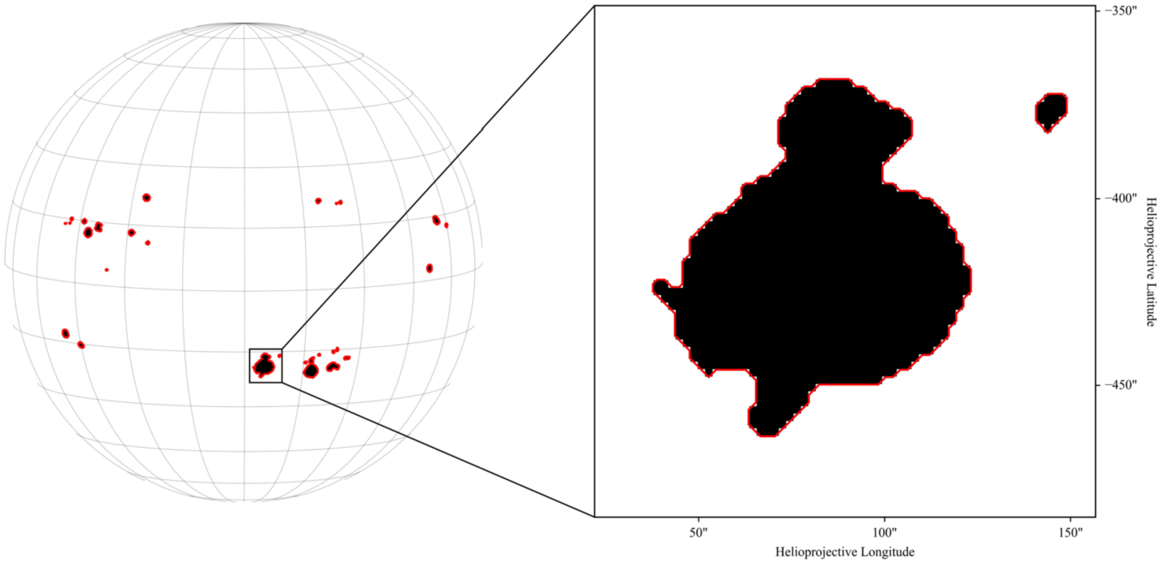

Figure 3 Solar disk map for September 26, 2001, at 17:50:33 UT, following transformation and binarization, displaying the tracked sunspots. The largest sunspot of the day is highlighted, with its total area (umbra + penumbra) outlined by the contour.

A practical application of our algorithm is illustrated in Figure 3, which shows a record from September 26, 2001, featuring a solar disk map with contoured sunspots. The image produced after applying the white top-hat transformation and inverted binarization clearly segments the sunspots, outlined in red. In this study, we only considered regions with an area greater than 16 squared pixels as valid sunspots, dismissing smaller points as false positives. The highlighted sunspot 9632, the largest of the day, had an estimated area of 960 millionths of the Sun's visible hemisphere, representing one of the largest events detected by our method.

2.7. Obtaining the Relative Sunspot Number

Following the detection of individual sunspots, the relative sunspot number can be calculated (Vanlommel et al. 2004; Hathaway 2015). The formula proposed by Rudolf Wolf at the Zurich Observatory in 1849, and widely used by the Solar Influences Data Analysis Center (SIDC), is defined as follows:

$$R = k(10g + s), \tag{3}$$

where s represents the number of individual sunspots observed, g is the number of observed sunspot groups and k is the personal correction coefficient introduced to account for variations among observers, observation sites, and instruments.

To calculate the number of sunspot groups, an automated method based on mathematical morphology was employed, similar to the approach described by Zhao et al. (2024). As illustrated in Figure 4, the process involves the following steps: After segmenting individual sunspots (Figure 4 (a)), the image is eroded using the same structuring element. This operation causes nearby dark regions to merge, forming larger areas (Figure 4 (b)). These areas are then contoured (Figure 4 (c)), and their number is counted. Figure 4 (d) shows the contoured groups projected onto the original solar map, along with the total number of groups.

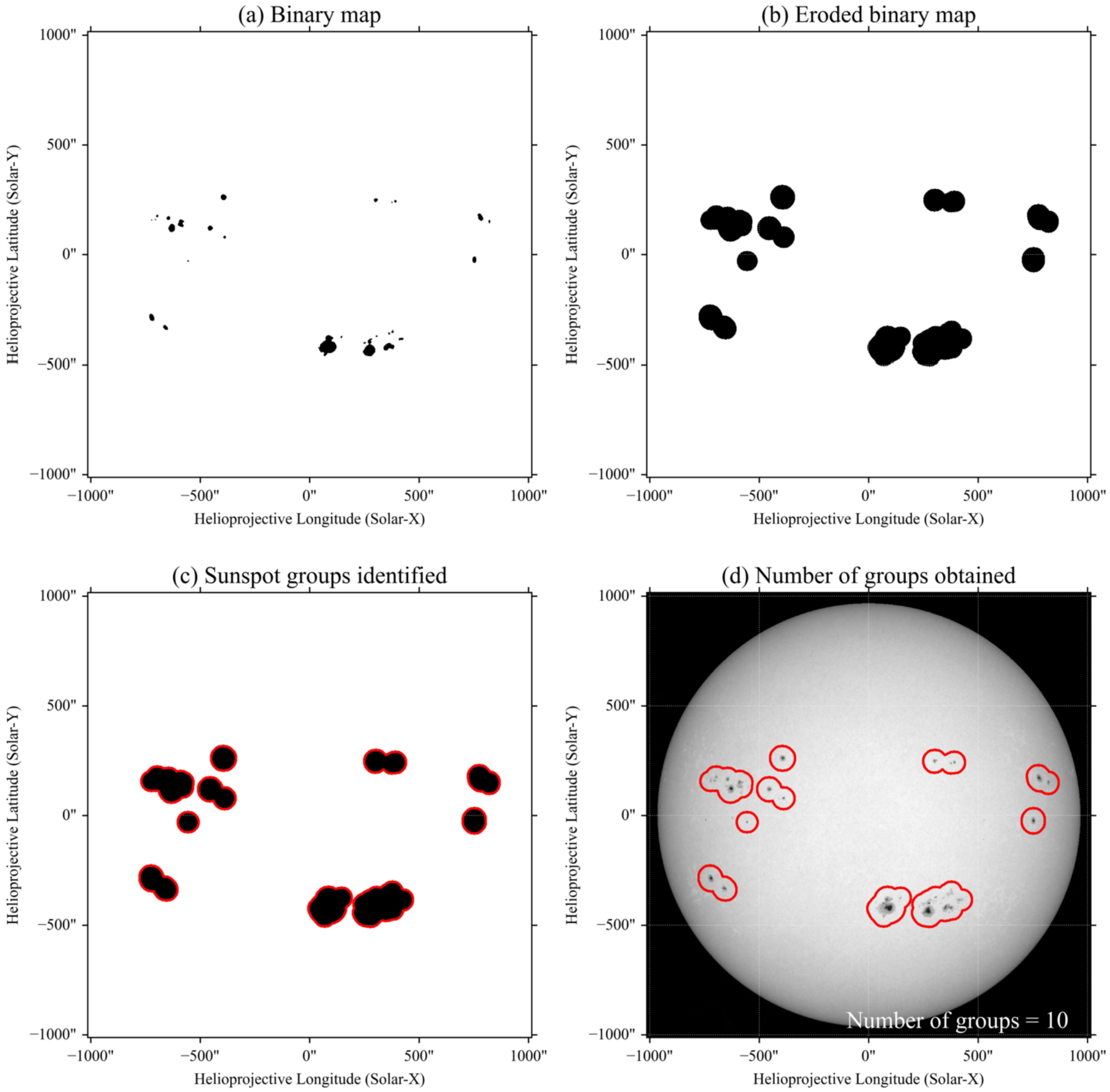

Figure 4 Process for identifying sunspot groups: (a) Solar disk map for September 26, 2001, following the white top-hat transformation and binarization steps. (b) Erosion of the map using the same structuring element. (c) Identification of the sunspot groups on the eroded map. (d) Projection of the identified groups and their counts onto the original solar map.

As noted by Clette et al. (2014), the coefficient k in the Wolf sunspot number (Equation 3) accounts for variations in observer skill and instrumentation, leading to a "relative" rather than absolute measure. To compensate for these differences and ensure comparability with established data, we calibrated k by comparing our PyMosT-derived sunspot numbers (assuming $k = 1$) with data from the Solar Influences Data Analysis Center (SIDC).[2]

Following the method described by Zhao et al. (2024), we employed a least-squares linear regression to compare our data with SIDC data. This analysis yielded a correlation coefficient and an angular coefficient of 1.97. Consequently, we set our personal correction coefficient k to 1.97 and applied this value in Equation 3 to calculate the relative sunspot number for our measurements.

[2]WDC-SILSO, Royal Observatory of Belgium, Brussels: https://www.sidc.be/silso/home.

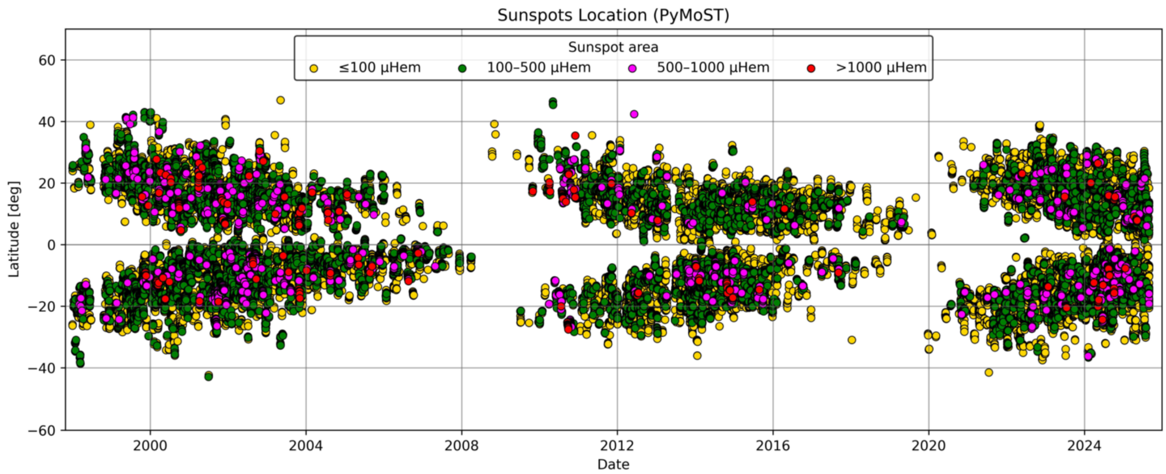

Figure 5 Representation of Mauder's Butterfly Diagram, with sunspot latitudes (in degrees) as a function of time (in years), referring to Cycles 23, 24 and the current stage of Cycle 25, with sunspot areas, represented by different colors, in millionths of the Sun's visible hemisphere, obtained using the PyMoST code.

3. Results and Discussion

The analysis of approximately 10,000 white-light solar disk images, covering the period from January 1, 1998, to August 28, 2025, using the PyMoST software, allowed for the identification and tracking of nearly 52,000 sunspots. The resulting dataset is provided in two CSV files, "Sunspots.cvs" and "Groups.csv," which are publicly available on GitHub.[3] This comprehensive dataset provided the necessary parameters to accurately determine heliographic coordinates and performs an in-depth morphological analysis of the sunspots. One significant result of this analysis is depicted in Figure 5, which presents a butterfly diagram showing the latitudinal distribution of sunspots over time, covering solar cycles 23 and 24, as well as the ongoing phase of cycle 25. The diagram also illustrates the sunspot areas in millionths of the Sun's visible hemisphere, offering a detailed perspective on the evolution of solar activity across these cycles. This analysis not only reinforces the cyclical nature of solar activity but also contributes valuable insights into the progression and characteristics of sunspot formations over more than two decades.

Consistent with the findings of Maunder (1903, 1904), Hathaway (2015), van Driel-Gesztelyi and Owens (2020), our results confirm that the onset of each solar cycle is marked by the emergence of sunspots (or sunspot groups) at higher latitudes, typically near 40°. The automated analysis carried out by PyMoST across Solar Cycles 23, 24 and 25 enabled the precise identification of these initial spots and tracked their gradual migration toward lower latitudes, ultimately converging near the Sun's equator as each cycle concludes. This well-reported migration pattern, represented in the "butterfly diagram", clearly illustrates the dynamics of solar activity across these cycles. Moreover, our results confirm the hemispheric asymmetry observed in Cycles 23 and 24, often referred to as "Active Hemispheres" by Hathaway (2015). This asymmetry, which is also evident in other indicators of solar activity such as faculae, prominences, and coronal brightness, underscores the complex and non-uniform nature of the Sun's magnetic activity.

Solar Cycle 24, spanning from 2009 to mid-2020, exhibited significantly lower solar activity compared to its predecessor, as illustrated in Figure 5. The variation in sunspot numbers between consecutive 11-year cycles is a well-documented phenomenon (Clette et al.

[3] https://github.com/grangeirodario/pymost.

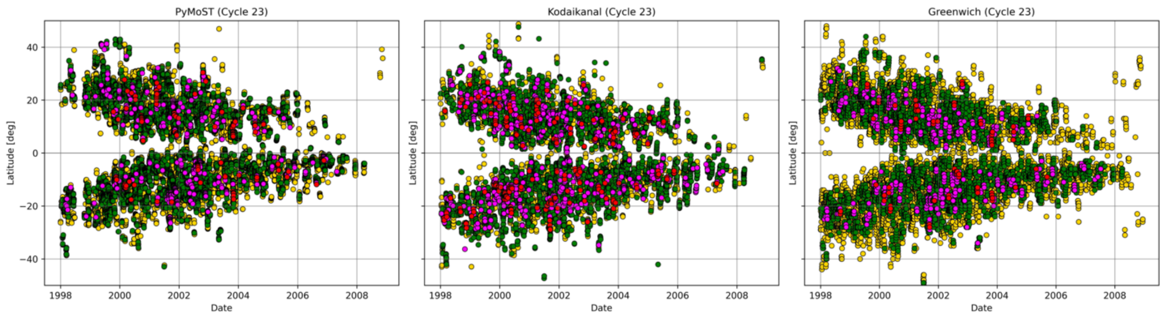

Figure 6 Comparison between the butterfly diagrams (position and area as a function of time) of sunspots for Solar Cycle 23, obtained by PyMoST (left), KSO (center) and RGO (right).

2014). However, Cycle 24 is particularly notable for its anomalously low sunspot count, a characteristic that has led several researchers to classify it as atypical (Pesnell 2016; Imada et al. 2020). This unusually low solar activity contrasts sharply with the trends observed over the past century, and its underlying causes remain a subject of ongoing investigation. The uncertainty regarding whether this reduced activity will persist in future cycles underscores the critical importance of sunspot prediction, despite the ongoing debates and varying results among different forecasting methods in the literature (Pesnell 2016).

To validate our methods, we compared the results obtained by PyMoST with reference data from the Royal Greenwich Observatory (RGO) and the Kodaikanal Solar Observatory (KSO). The RGO has been monitoring and recording sunspot areas since 1874, using its own measurements and those of its partner observatories in Cape Town, Kodaikanal and Mauritius (Hathaway 2015). This data, available up to 2016 on the observatory's website,[4] provides a solid basis for comparison. The KSO has been observing the Sun since 1904, using photographic plates (Mandal et al. 2017). In their paper, Mandal et al. (2017) digitized and calibrated this data, applying a sunspot tracking algorithm to generate a valuable time series for our comparative analysis.

A temporal comparison between sunspot position and sunspot area for Solar Cycle 23 is shown in Figure 6. In this figure, only the data for Solar Cycle 23 has been plotted, as this is the only complete solar cycle available in both databases. For comparison purposes, we limited the PyMoST and RGO data (which extends until mid-2016) to the final period of the KSO data, which covers until the end of 2011.

With regard to the position of sunspots, the results obtained by PyMoST show a solar cycle with characteristics of size, shape and pattern similar to those observed by KSO and RGO, as can be seen in Figure 6. However, we observed some differences in the number of sunspots compared to the RGO and in the areas of the spots compared to the KSO. Figure 7 shows a comparison of the sunspot areas obtained by PyMoST (red) with the KSO (black) and RGO (blue) data for the southern hemisphere (left), the northern hemisphere (center), and the entire disk (right). The subtle differences in sunspot areas can be attributed to factors such as detection and tracking methodologies, the quality of the images used, and possible observation biases.

In Figure 7 (a), we present a detailed comparison of the total daily sunspot areas as recorded by PyMoST, alongside reference data from the RGO and KSO. Overall, we observed strong agreement across the entire solar disk. However, hemispheric comparisons revealed discrepancies, particularly in the northern hemisphere, where PyMoST data diverged

[4] Royal Observatory, Greenwich - USAF/NOAA Sunspot Data: https://solarscience.msfc.nasa.gov/greenwch.shtml.

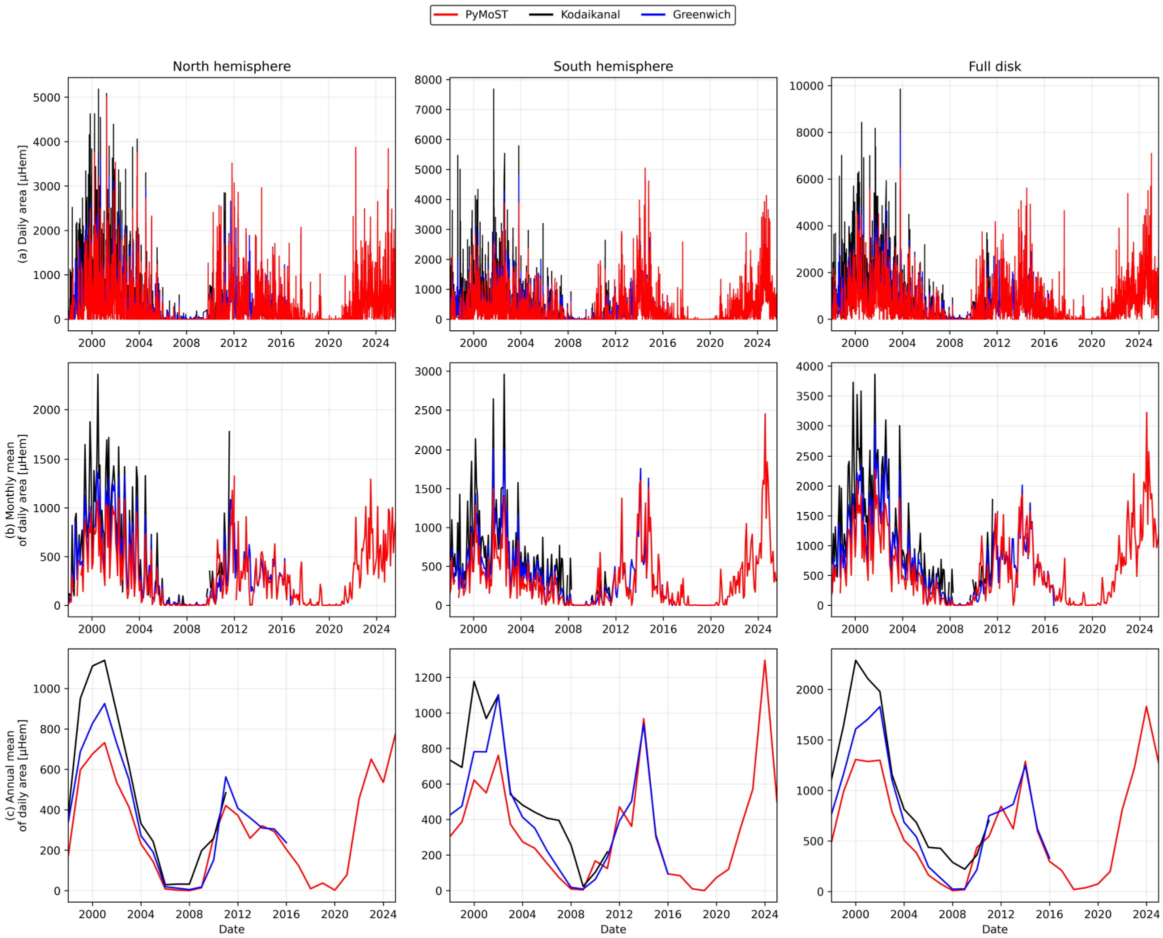

Figure 7 Comparison of the total sunspot areas obtained by PyMoST (red), KSO (black) and RGO (blue) for Solar Cycle 23. (a) Daily total areas for each hemisphere and full disk. (b) Monthly averages for each hemisphere and full disk. (c) Annual averages for each hemisphere and full disk.

from RGO and KSO data during the latter half of Solar Cycle 23 and the solar minimum phase. These divergences were more pronounced in the southern hemisphere, beginning earlier and persisting throughout the solar minimum, especially compared to KSO data.

Figure 7 (b) demonstrates a strong correlation between the monthly averages of total sunspot areas from PyMoST and the reference datasets during overlapping periods. Although some localized differences are observed in Cycles 23 and 24, especially in the southern hemisphere, the overall agreement between the datasets underscores the robustness of our method. In contrast, Figure 7 (c), which depicts the annual averages of the total sunspot areas, reveals divergences between the PyMoST and RGO data for both hemispheres, despite the good relationship with the KSO data.

Despite the subtle divergences observed, especially in the separate hemispheres, our data (PyMoST) shows a strong correlation with the RGO and KSO data, both in terms of sunspot position and area. It is important to note that these discrepancies can be attributed to several factors. In the case of the RGO, the combination of measurements from different observatories around the world (Cape Town, Kodaikanal and Mauritius), with different scales and instruments, can introduce variations in the results (Hathaway 2015). The KSO data, obtained by digitizing photographic plates and applying a semi-automated algorithm (Imada et al. 2020), may have detection biases due to the conditions of the plates and the nature of the algorithm, contributing to the differences observed. However, the general consistency

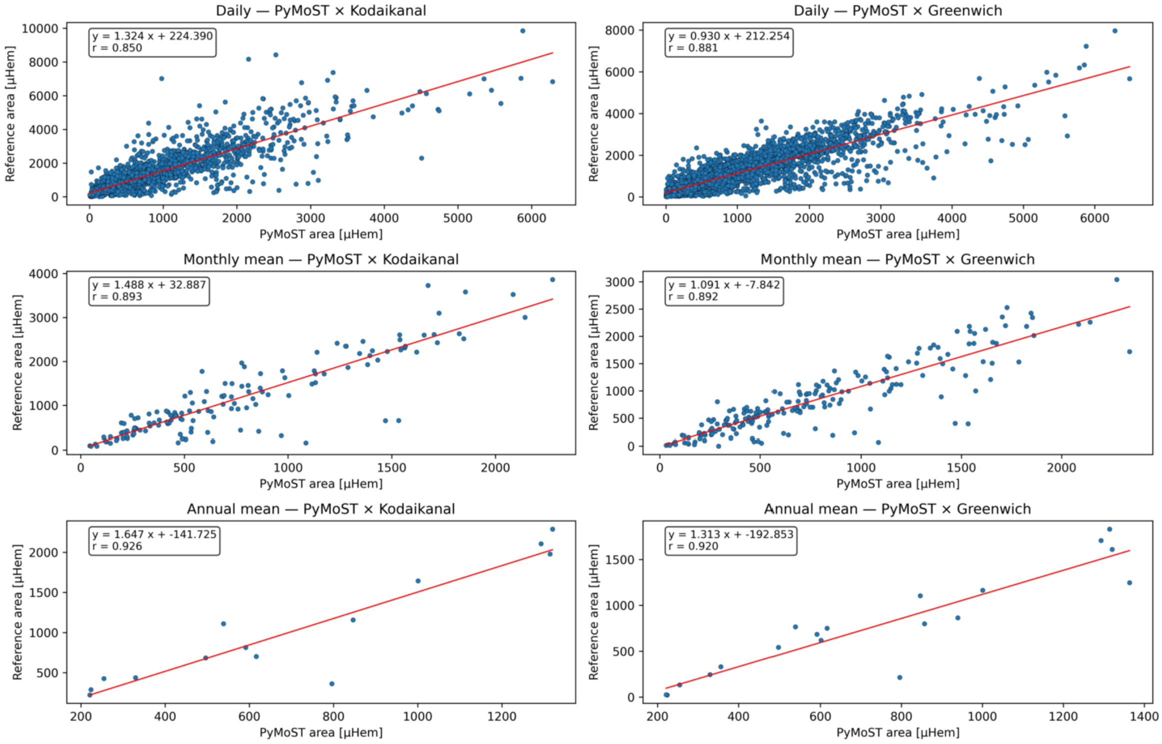

Figure 8 Correlation between sunspot areas obtained by PyMoST and RGO (left column) and also KSO (right column) data for the period January 1, 1998, to August 2, 2011. The scatter plots show: (top) daily total areas, (middle) monthly averages and (bottom) annual averages. Each graph includes the least squares linear fit coefficients (red line) and Pearson's correlation coefficient.

between the data sets reinforces the validity and reliability of PyMoST as a tool for analyzing solar activity.

To assess the correlation between sunspot area measurements, we analyzed data from January 1, 1998, to August 2, 2011, a period where the three datasets (PyMoST, RGO, and KSO) overlap. Figure 8 presents scatter plots, each with a least squares line fitting and corresponding Pearson correlation coefficients, comparing total daily sunspot area (Figure 8 (top), monthly averages (Figure 8 (middle)), and annual averages across the full solar disk (Figure 8 (bottom)). The results indicate a strong correlation between the PyMoST results and those from the RGO and KSO observatories, underscoring the consistency and reliability of our methods for sunspot detection and tracking.

Analysis of the total daily sunspot areas revealed a strong correlation between the PyMoST data and that of the KSO and RGO reference observatories (r = 0.850 and 0.881, respectively). The angular coefficients of the fitting lines (1.324 for KSO and 0.93 for KSO) demonstrate an almost linear correlation between the areas calculated by PyMoST and those measured by the observatories, with a slight tendency to overestimate in relation to KSO. Despite a systematic shift of approximately 200 μHem between the data, this high correlation demonstrates PyMoST's ability to capture the dynamics of sunspot area variation over time.

When examining the monthly averages of total sunspot areas, our analysis demonstrated an even stronger correlation (r = 0.893 with KSO and r = 0.892 with RGO), highlighting increased consistency across the datasets over time. The angular coefficients of the fitting lines (1.488 for KSO and 1.091 for RGO) further emphasize the near-linear relationship between the monthly averages, with a slight overestimation relative to KSO, similar to the trend observed in the daily data. The systematic shift, while present, remains relatively small (32.887

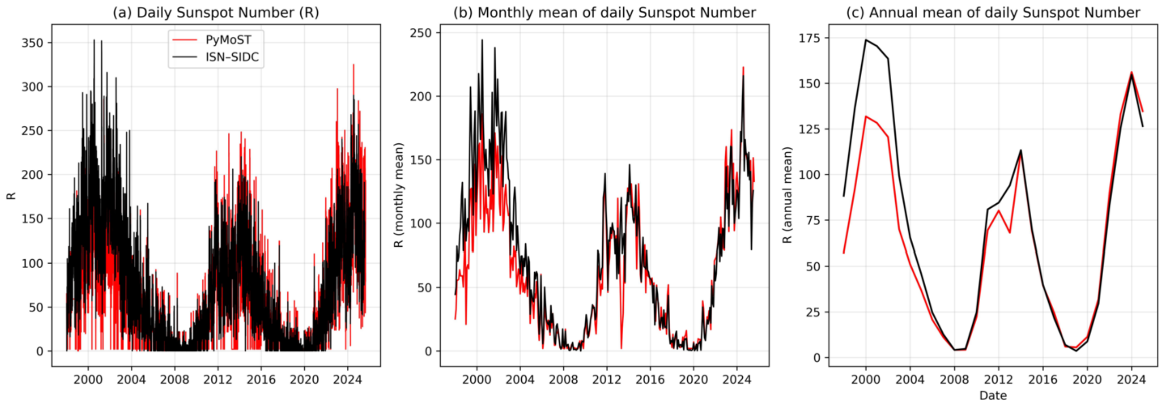

Figure 9 Relative number of PyMoST sunspots compared to the International Sunspot Number - SIDC, for the period 1998 to mid-2024. (a) Total daily sunspot number. (b) Monthly average of the total daily sunspot number. (c) Annual average of the total daily sunspot number.

for KSO and 7.842 for RGO), especially when considering monthly averages. This indicates the robustness of PyMoST in accurately capturing the monthly variations in sunspot areas.

We concluded the analysis of the annual averages of total sunspot areas, finding the highest correlations between the PyMoST data and those from the reference observatories ($r = 0.926$ for KSO and $r = 0.920$ for RGO). The angular coefficients of the fitting lines (1.647 for KSO and 1.313 for RGO) further validate the nearly linear relationship between the annual averages, with a slight tendency to overestimate in relation to KSO. The systematic shift in this context is -141.725 for KSO and -192.853 for RGO, compared to the magnitude of the annual areas, underscoring the high accuracy of PyMoST in estimating the annual average sunspot areas.

In addition to the previous findings, Figure 9 also presents the temporal evolution of the relative sunspot numbers, comparing the PyMoST results (in red) with the International Sunspot Number from SIDC (in black) over the entire period analyzed by PyMoST (1998 to mid-2025). Figure 9 (a) depicts the total daily sunspot numbers, which demonstrate a remarkable correlation with the SIDC data, consistently reflecting the approximate 11-year solar cycle in both cases. However, some variations are evident. The PyMoST data exhibit greater variability, with sunspot maxima occasionally surpassing those reported by SIDC, indicating a potential sensitivity to smaller or more transient sunspot groups.

Figure 9 (b) illustrates the monthly averages of total sunspot numbers, further confirming the overall trend observed in comparison with the SIDC data. The use of monthly averages helps mitigate some of the daily fluctuations seen in plot (a), providing a clearer depiction of the solar cycles and making long-term variations across the analyzed cycles more apparent. The discrepancies between the datasets are notably reduced when considering the monthly averages, suggesting that the daily variations tend to balance out over longer periods. Furthermore, the alignment of peak activity periods between the two datasets reinforces the effectiveness and reliability of our method.

Figure 9 (c) presents the annual averages of the total daily sunspot numbers. These annual averages provide an even smoother dataset, accentuating the discrepancies between PyMoST and SIDC, particularly during periods of maximum solar activity, where PyMoST tends to show slightly lower peaks than those recorded by SIDC, though the overall trends remain consistent. Despite these differences, the analysis demonstrates a strong correlation between the sunspot counts, confirming the robustness of PyMoST in detecting and quantifying solar activity. This high level of agreement underscores the utility of PyMoST as a reliable tool for solar activity studies, capable of producing results that align closely with internationally recognized reference data.

Overall, both datasets exhibit consistent trends that correlate well over time. The occasional discrepancies can be attributed to the different methodologies used for counting sunspots in the two databases. In conclusion, the results presented here underscore the effectiveness of PyMoST in accurately detecting, tracking, and characterizing sunspots, paving the way for new advancements in solar physics research and enhancing our understanding of the Sun's activity cycles.

4. Conclusion

In this study, we introduce PyMoST, an automated sunspot tracking method developed in the Python language. The approach based on segmentation by mathematical morphology has demonstrated high efficiency in the accurate detection of sunspots, determining their area and number in an extensive series of images of the solar disk, covering several years of observations.

The results obtained by PyMoST provide critical insights into solar parameters essential for understanding solar magnetic activity. Our analysis of the position, shape, and amplitude of sunspots across Solar Cycles 23, 24, and the current phase of Cycle 25 aligns with previous research, notably reinforcing Spörer's Law of Zones and demonstrating the robustness and precision of our method.

PyMoST's capability to produce daily and monthly sunspot area metrics has shown strong correlation with solar cycle patterns. The exceptional agreement between our results and those from the Royal Greenwich Observatory, Kodaikanal Solar Observatory, and other literature highlights the reliability of PyMoST. Furthermore, the close correlation between the average monthly sunspot numbers from PyMoST and the International Sunspot Number (SIDC) underscores the method's efficacy in recording and comparing sunspot numbers.

Our validation also extends to the detection of asymmetry in solar activity between hemispheres, a pattern consistent with findings from Hathaway (2015) and van Driel-Gesztelyi and Owens (2020), and corroborated by our results. This study significantly contributes to the field of solar physics by providing a robust, validated, and automated sunspot tracking method. PyMoST's ability to handle large datasets autonomously and its accuracy in relation to reference data pave the way for enhanced understanding of solar magnetic activity and its effects on the solar system. By complementing existing research efforts, PyMoST serves as a valuable tool for advancing our understanding of solar dynamics and improving research in solar physics.

Appendix: Equivalence Between FITS and JPEG2000 Data

The methodological validation of the dataset used in this study included additional tests comparing images obtained from the Helioviewer repository and the JSOC (Joint Science Operations Center). Although both sources provide observations from the same instruments (SOHO/MDI and SDO/HMI), differences in file formats and preprocessing procedures could, in principle, influence the outcome of the processing pipeline. The analysis presented in this appendix demonstrates that such differences do not lead to significant variations once the full processing workflow adopted in this study is applied, thereby ensuring the robustness and reproducibility of the measurements.

To perform this validation, two representative cases were selected, one for each instrument analyzed: (i) an MDI observation (SOHO/MDI), and (ii) an HMI observation (SDO/HMI). The FITS images corresponding to the MDI and HMI instruments were retrieved directly from JSOC using the Fido interface of the SunPy package, as illustrated below for the MDI instrument (for the HMI case, it is sufficient to modify the date and the `jsoc.Series` parameter to “`hmi.Ic_720s`”:)

```

from sunpy.net import Fido, attrs as a

t_start = "2001-09-26T17:50:33"
t_end = "2001-09-26T17:50:33"

result = Fido.search(
    a.Time(t_start, t_end),
    a.jsoc.Series("mdi.fd_Ic"),
    a.jsoc.Notify("dario.grangeiro@aluno.ufca.edu.br"),
)

files = Fido.fetch(result)
fit_map = Map(files[0])
```

After downloading, the FITS files were subjected to an intensity normalization procedure to ensure proper comparability with the JPEG2000 images from Helioviewer, which inherently include prior scaling and compression steps. The normalization was performed as illustrated in the following code snippet:

```

data = np.nan_to_num(fit_map.data, nan=0.0)
min_val = np.nanmin(data)
max_val = np.nanmax(data)
normalized_data = (data - min_val) / (max_val - min_val)
scaled_data = (normalized_data * 255).astype(np.uint8)
```

The rationale for this normalization is to ensure that the intensity values in the FITS files—originally expressed in physical units that differ between instruments—are rescaled to a standardized range ($0-255$). This guarantees that both image sets—JSOC/FITS and Helioviewer/JPEG2000—can be processed by the same sunspot detection pipeline without instrumental or numerical differences affecting contrast, segmentation, or the photometric metrics used.

After this step, the images were subjected to the same processing workflow described in the main body of the article, including heliographic projection and sunspot segmentation. Following processing, both datasets produced consistent solar disk images, with no detectable structural differences in the resulting intensity maps or segmented regions, as shown in Figure 10.

Moreover, the quantitative parameters extracted from each source, specifically the heliographic latitude and longitude of the detected sunspots, as well as their projected areas, were found to be statistically indistinguishable in both cases, with the exception of a single sunspot detected in the FITS image from 2013-04-06 (HMI series) that was not detected in the corresponding JPEG2000 image for the same date. The results are illustrated in Figure 11; the horizontal shift in the plot is solely due to the absence of this data point in the JPEG2000 dataset.

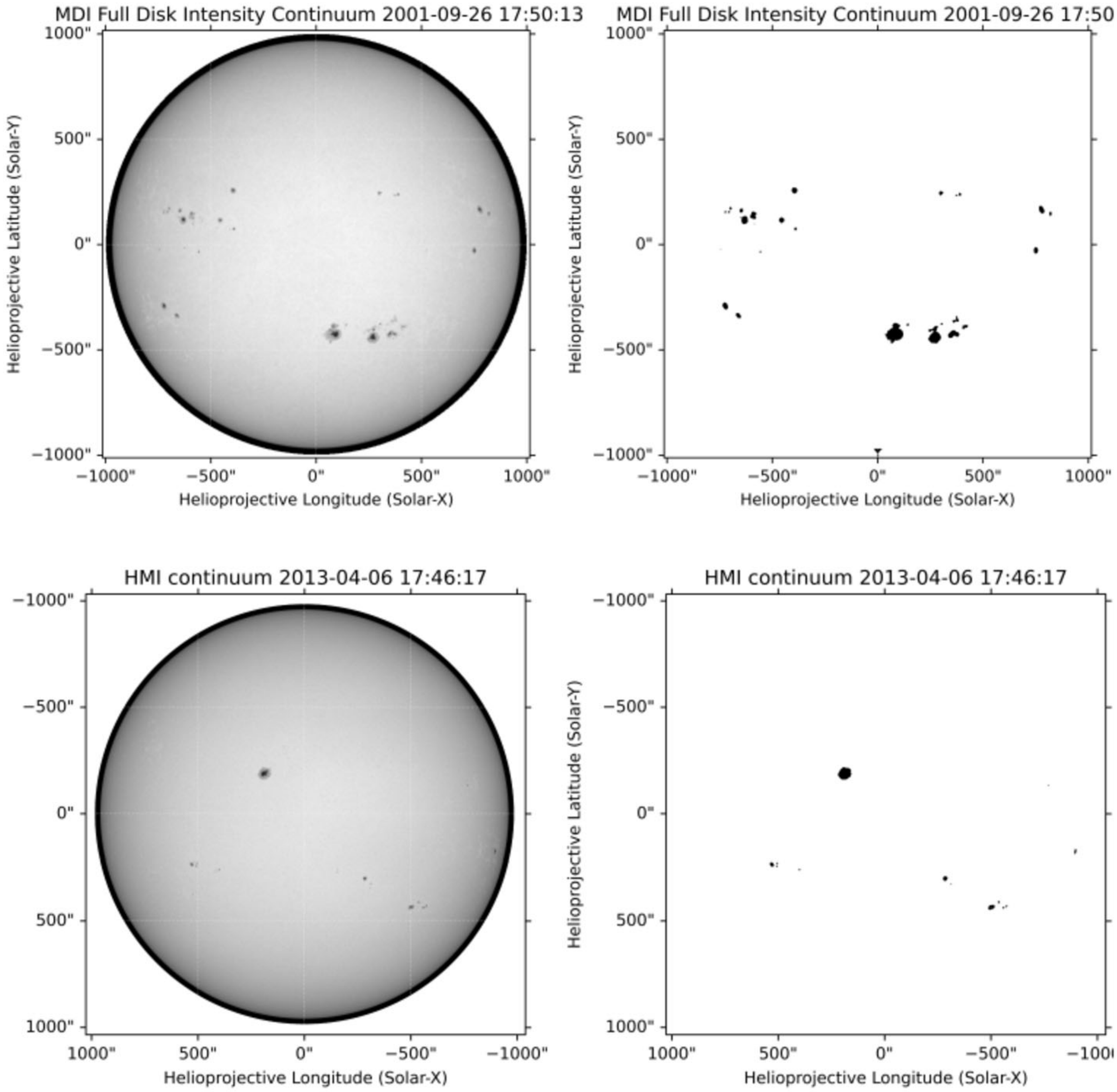

Figure 10 Comparison of the processed products from the MDI (2001-09-26) and HMI (2013-04-06) observations. The panels on the left display the continuum intensity images after heliographic reprojection, whereas the panels on the right show the segmented regions corresponding to the identified sunspots. It is evident that both datasets yield consistent intensity maps and segmentations, with no perceptible structural differences between the applied techniques.

The results obtained showed excellent agreement between the two data sources for both instruments (MDI and HMI). The discrepancies identified remain within the expected uncertainties for solar data and do not affect the scientific interpretation.

Furthermore, these tests confirm that the JSOC and Helioviewer data become scientifically equivalent once the standardized processing adopted in this study is applied. Therefore, both repositories can be used interchangeably for the detection and characterization of sunspots, reinforcing the methodological robustness and reliability of the analyses provided.

Acknowledgments The authors, C. D. Grangeiro e T. S. S. Duarte, would like to thank the following institutions: Universidade Federal do Cariri – Instituto de Formação de Educadores (IFE/UFCA) and Fundação Cearense de Apoio ao Desenvolvimento Científico e Tecnológico (Funcap) for their financial support; and author H. R. Coelho thanks the Conselho Nacional de Desenvolvimento Científico e Tecnológico (CNPq) for financial support. We thank the anonymous reviewer for very useful comments that helped to greatly improve the manuscript.

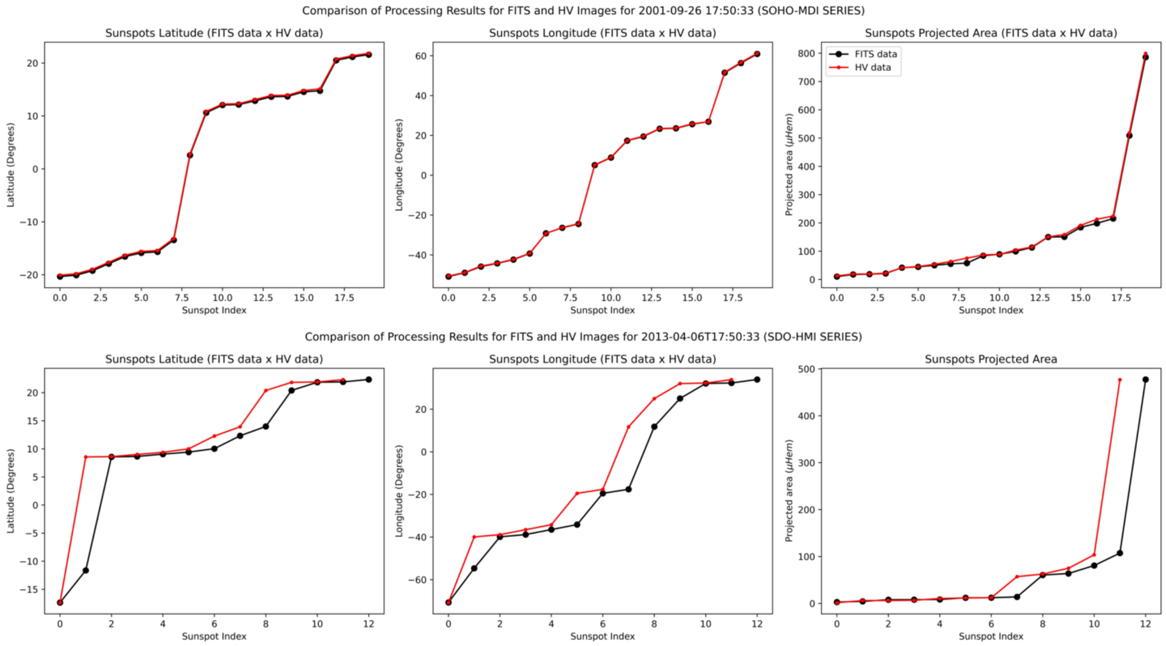

Figure 11 Comparison of the quantitative sunspot parameters obtained from the FITS and JPEG2000 images for the dates 2001-09-26 (SOHO/MDI) and 2013-04-06 (SDO/HMI). The plots show, for each detected sunspot, the heliographic latitudes and longitudes, as well as the projected areas derived from both datasets. A high level of agreement is observed between the measurements, with statistically negligible differences, except for the absence of one sunspot in the JPEG2000 image from 2013-04-06, which leads to the visible offset in the corresponding plots.

Author contributions C.D.G. conducted the mathematical morphology research, developed the PyMoST code, acquired the data, authored the primary text, and created the figures. T.S.S.D., as both author and supervisor, contributed to the main text, conducted result analysis and discussion, and provided overall guidance. J.S.C., J.F.O.J. and J.D.N.J. contributed to the analysis and discussion of the results and provided critical revisions to the manuscript. H.R.C. was responsible for reviewing the work and refining the English language throughout the manuscript.

Data availability The code and data have been deposited in the GitHub repository and archived in Zenodo, generating the DOI, which has been duly cited in the manuscript (last paragraph of page 2).

Declarations

Competing interests The authors declare no competing interests.

References

Banfield, J.D., Raftery, A.E.: 1992, Ice floe identification in satellite images using mathematical morphology and clustering about principal curves. *J. Am. Stat. Assoc.* **87**, 7. DOI.

Bloch, I., Heijmans, H., Ronse, C.: 2007, Mathematical morphology. In: *Handbook of Spatial Logics*, Springer, Berlin, 857. DOI.

Bourgeois, S., Barata, T., Erdélyi, R., Gafeira, R., Oliveira, O.: 2024, Sunspots identification through mathematical morphology: the method. *Sol. Phys.* **299**, 10. DOI. ADS.

Bradski, G.: 2000, The OpenCV library. *Dr. Dobb's J. Softw. Tools Prof. Program.* **25**, 120.

Carrington, R.C.: 1863, *Observations of the spots on the Sun: from November 9, 1853, to March 24, 1861, made at Redhill*, Williams and Norgate. ADS.

Carvalho, S., Gomes, S., Barata, T., Lourenço, A., Peixinho, N.: 2020, Comparison of automatic methods to detect sunspots in the Coimbra Observatory spectroheliograms. *Astron. Comput.* **32**, 100385. DOI. ADS.

Chola, C., Benifa, J.B.: 2022, Detection and classification of sunspots via deep convolutional neural network. *Glob. Transit. Proc.* **3**, 177. DOI. ADS.
Clette, F., Svalgaard, L., Vaquero, J.M., Cliver, E.W.: 2014, Revisiting the sunspot number: a 400-year perspective on the solar cycle. *Space Sci. Rev.* **186**, 35. DOI. ADS.
Curto, J.J., Blanca, M., Martínez, E.: 2008, Automatic sunspots detection on full-disk solar images using mathematical morphology. *Sol. Phys.* **250**, 411. DOI. ADS.
El Abbadi, N.K., Al Saadi, E.H.: 2013, Blood vessels extraction using mathematical morphology. *J. Comput. Sci.* **9**, 1389. DOI.
Goel, S., Mathew, S.K.: 2014, Automated detection, characterization, and tracking of sunspots from SoHO/MDI continuum images. *Sol. Phys.* **289**, 1413. DOI. ADS.
Grangeiro, D.: 2025, PyMoST: Python Morphological Sunspot Tracker. DOI. https://github.com/grangeiro-dario/pymost.
Hale, G.E., Ellerman, F., Nicholson, S.B., Joy, A.H.: 1919, The magnetic polarity of sun-spots. *Astrophys. J.* **49**, 153. DOI. ADS.
Haralick, R.M., Sternberg, S.R., Zhuang, X.: 1987, Image analysis using mathematical morphology. *IEEE Trans. Pattern Anal. Mach. Intell.* 532. DOI.
Hathaway, D.H.: 2015, The solar cycle. *Living Rev. Sol. Phys.* **12**, 4. DOI. ADS.
Imada, S., Matoba, K., Fujiyama, M., Iijima, H.: 2020, Solar cycle-related variation in solar differential rotation and meridional flow in solar cycle 24. *Earth Planets Space* **72**, 182. DOI. ADS.
Klingler, J.W., Vaughan, C.L., Fraker, T., Andrews, L.T.: 1988, Segmentation of echocardiographic images using mathematical morphology. *IEEE Trans. Biomed. Eng.* **35**, 925. DOI.
Mandal, S., Hegde, M., Samanta, T., Hazra, G., Banerjee, D., Ravindra, B.: 2017, Kodaikanal digitized white-light data archive (1921-2011): analysis of various solar cycle features. *Astron. Astrophys.* **601**, A106. DOI. ADS.
Matheron, G.: 1975, *Random Sets and Integral Geometry*.
Maunder, E.W.: 1903, Spoerer's law of zones. *Observatory* **26**, 329. ADS.
Maunder, E.W.: 1904, Note on the distribution of sun-spots in heliographic latitude, 1874-1902. *Mon. Not. R. Astron. Soc.* **64**, 747. DOI. ADS.
Meadows, P.: 2002, The measurement of sunspot area. *J. Br. Astron. Assoc.* **112**, 353. ADS.
Morales, S., Naranjo, V., Angulo, J., Alcañiz, M.: 2013, Automatic detection of optic disc based on PCA and mathematical morphology. *IEEE Trans. Med. Imaging* **32**, 786. DOI.
Mumford, S.J., Christe, S., Pérez-Suárez, D., Ireland, J., Shih, A.Y., Inglis, A.R., Liedtke, S., Hewett, R.J., Mayer, F., Hughitt, K., et al.: 2015, SunPy—Python for solar physics. *Comput. Sci. Discov.* **8**, 014009.
Mumford, S.J., Freij, N., Stansby, D., Christe, S., Shih, A.Y., Ireland, J., Mayer, F., Hughitt, V.K., Ryan, D.F., Liedtke, S., et al.: 2025. Sunpy: a Core Package fOr Solar Physics, Zenodo. DOI
Najman, L., Talbot, H.: 2013, *Mathematical Morphology: From Theory to Applications*, Wiley, New York.
Pesnell, W.D.: 2016, Predictions of solar cycle 24: how are we doing? *Space Weather* **14**, 10. DOI. ADS.
Price-Whelan, A.M., Sipőcz, B., Günther, H., Lim, P., Crawford, S., Conseil, S., Shupe, D., Craig, M., Dencheva, N., Ginsburg, A., et al.: 2018, The astropy project: building an open-science project and status of the v2. 0 core package. *Astron. J.* **156**, 123.
Roslan, R., Jamil, N., Mahmud, R.: 2010, Skull stripping of MRI brain images using mathematical morphology. In: *2010 IEEE EMBS Conference on Biomedical Engineering and Sciences (IECBES)* **26**, IEEE Press, New York. DOI.
Santos, J., Peixinho, N., Barata, T., Pereira, C., Coimbra, A.P., Crisóstomo, M.M., Mendes, M.: 2023, Sunspot detection using YOLOv5 in spectroheliograph H-alpha images. *Appl. Sci.* **13**, 5833. DOI.
Schwabe, H.: 1844, Sonnenbeobachtungen im jahre 1843. Von Herrn Hofrath Schwabe in Dessau. *Astron. Nachr.* **21**, 233. DOI. ADS.
Serna, A., Marcotegui, B.: 2014, Detection, segmentation and classification of 3D urban objects using mathematical morphology and supervised learning. *ISPRS J. Photogramm. Remote Sens.* **93**, 243.
Serra, J.: 1982, *Image Analysis and Mathematical Morphol-Ogy*. DOI.
Soille, P., et al.: 1999, *Morphological Image Analysis: Principles and Applications* **12**, Springer, Berlin. DOI.
The SunPy Community, Barnes, W.T., Bobra, M.G., Christe, S.D., Freij, N., Hayes, L.A., Ireland, J., Mumford, S., Perez-Suarez, D., Ryan, D.F., Shih, A.Y., Chanda, P., Glogowski, K., Hewett, R., Hughitt, V.K., Hill, A., Hiware, K., Inglis, A., Kirk, M.S.F., Konge, S., Mason, J.P., Maloney, S.A., Murray, S.A., Panda, A., Park, J., Pereira, T.M.D., Reardon, K., Savage, S., Sipőcz, B.M., Stansby, D., Jain, Y., Taylor, G., Yadav, T., Rajul, D.T.K.: 2020, The SunPy Project: Open Source Development and Status of the Version 1.0 Core Package. *Astrophys. J.* 890. DOI.
Thompson, W.T.: 2006, Coordinate systems for solar image data. *Astron. Astrophys.* **449**, 791. DOI. ADS.
van Driel-Gesztelyi, L., Owens, M.J.: 2020, Solar cycle. *Oxford Res. Encycl. Phys.* DOI.
Vanlommel, P., Cugnon, P., Linden, R.A.M.V.D., Berghmans, D., Clette, F.: 2004, The sidc: world data center for the sunspot index. *Sol. Phys.* **224**, 113. DOI. ADS.

Vourlidas, A.: 2021, Improving the medium-term forecasting of space weather: a big picture review from a solar observer's perspective. *Front. Astron. Space Sci.* **8**, 68. DOI. ADS.

Watson, F.T., Fletcher, L., Marshall, S.: 2011, Evolution of sunspot properties during solar cycle 23. *Astron. Astrophys.* **533**, A14. DOI.

Zhao, C., Yang, S., Wang, T., Zhao, H., Liu, S., He, F., Hu, Z.: 2024, An automatic approach for grouping sunspots and calculating relative sunspot number on SDO/HMI continuum images. *Astron. J.* **167**, 52. DOI.

Zharkov, S., Zharkova, V., Ipson, S., Benkhalil, A.: 2004, Automated recognition of sunspots on the soho/mdi white light solar images. In: *Knowledge-Based Intelligent Information and Engineering Systems: 8th International Conference, KES 2004, Proceedings*, Part III, 8, **446** *Wellington, New Zealand*, *September 20 – 25, 2004*. Springer, Berlin. DOI.

DECLARAÇÃO

Declaro para os devidos fins que este Trabalho de Conclusão de Curso, apresentado na modalidade de artigo completo aceito para publicação em revista científica com Qualis na área de estudo (conforme o Art. 9º, § 2º, da Resolução do Trabalho de Conclusão de Curso, no âmbito do curso de Licenciatura em Física do Instituto de Formação de Educadores da Universidade Federal do Cariri), foi desenvolvido sob minha orientação e encontra-se em sua versão final.

Informo também que procedi à revisão final do documento, constatando que atende às especificações das normas da ABNT para apresentação de trabalhos acadêmicos da UFCA, no que diz respeito ao conteúdo e à formatação aplicáveis a esta modalidade.

gov.br
Documento assinado digitalmente
GILSON FRANCISCO DE OLIVEIRA JUNIOR
Data: 31/08/2026 14:39:09-0300
Verifique em https://validar.iti.gov.br

Assinatura do(a) Orientador(a)

Gilson Francisco de Oliveira Junior